

GT2011-4599,

TURBOMACHINERY THERMAL ANALYSIS USING COUPLED TWO- AND THREE DIMENSIONAL MODELS AND REDUCED ORDER FLUID MODELS

Jesus Contreras, Roque Corral* and Guillermo Pastor

Technology and Methods Department
Industria de TurboPropulsores S.A.
28830 Madrid, Spain

e-mails: Jesus.Contreras@itp.es, Roque.Corral@itp.es, Guillermo.Pastor@itp.es

ABSTRACT

A methodology to couple two- and three dimensional thermal models is described. The method uses reduced order fluid models as a mechanism to transfer heat fluxes and average temperatures at the interface. In particular the concept of a duct-void is introduced to ease the coupling of different types of models. A new edge-based thermal solver, which is used in this process, is briefly described. A realistic case, corresponding to a two-stage turbine, is used to illustrate the usefulness of the method. It is concluded that the temperature difference between a fully coupled approach and a simpler unidirectional method (in which a two-dimensional global model is first computed and, then, the temperatures at the interface are transferred to three-dimensional sub-components) may be large enough to affect engineering decisions.

NOMENCLATURE

A area pointing outward to the boundary.
 A_l wet area per length unit.
 c_p fluid specific heat at constant pressure.
 c_v fluid specific heat at constant volume.
 c specific heat for solids.
CFD Computational Fluid Dynamics code.
CPU Central Processing Unit
 ϵ radiating emissivity of a gray body.
 $f_{i \rightarrow j}$ view factor of j as seen from i .

h convective heat transfer coefficient.
HTC heat transfer coefficient.
 k thermal conductivity at solids.
 \dot{m} mass flow.
 Ω solid domain.
 Q Volumetric heat source
 Q_l total heat per length unit.
 Q heat.
 q heat flux.
 ρ density.
RAM Random Access Memory
 R thermal resistance.
 Σ solid boundary.
 σ Stefan-Boltzmann constant.
SOR Successive Over-Relaxation scheme.
 s arc length.
 T_w local temperature at solid walls.
 T_∞ fluid bulk temperature.
Subscripts/superscripts
 ∞ fluid bulk conditions.
 i, j node indices.
 s Stream bulk conditions.
 w solid wall.

INTRODUCTION

Gas turbines operate in an aggressive thermal environment. Main flow-path transfers heat by convection to airfoils, casings and eventually disks. Heat is diffused by conduction from the surface

*Also associate professor at the Department of Engine Propulsion and Fluid Dynamics of the School of Aeronautics, UPM

to the inner part of the turbine components and further to other components by contact. When the surface temperature is large enough radiation may play a relevant role also, making the problem even more complex. Heat transfer analysis of a whole gas turbine, or even of one of its modules, involves tens or hundreds of components, which makes the problem even more complex from a logistic point of view.

Ideally, a fully-coupled 3D unsteady thermo-fluid-mechanical model of the whole turbine could be set up and solved. However there are several bottlenecks (e.g.: pre-processing and computing time) that make such solution not compatible with the current design timescales. A hierarchical approach is followed in practice. First Computational Fluid Dynamics (CFD), 0D and 1D fluid network models are constructed. Today a huge effort is devoted to the development of efficient coupling methods between the fluid and solid domains [1, 2, 3]. The motivation behind this effort is the pursue of higher fidelity models that may eventually increase the accuracy of the predictions.

On the solid part a 2D/Q3D thermal model of the whole turbine, with different types of boundary conditions to take into account convection using simple models, and even radiation effects if needed, is first constructed. The output of this model are turbine metal temperatures and displacements which are used as boundary conditions for 3D detail models. This type of modeling has a clear directional effect since usually there is no feedback of the 3D sub-models to the Q3D global models. Alternatively full 3D models of the whole turbine could be constructed but this is by no means an easy task in practice. An example of such a similar methodology is shown at [4].

Here we propose a new approach in which two- and three dimensional models are linked in a fully consistent way. The method allows the use of complex three-dimensional sub-components on demand, while keeping the modeling complexity at a low profile there where axi-symmetric models suffice. This approach is believed to be a good compromise between increase accuracy and additional modeling effort.

The paper first presents a description of the thermal solver with a brief outline of the different types of boundary conditions that are supported. Then a description of the new methodology and the tools needed for its practical implementation are presented and applied to the analysis of a two-stage turbine. Finally the results of the application of the approach are compared against the classical approach.

The solver itself, the methodology and the conclusions derived from its application presented in this work are believed to be original since it is difficult, in practice, to set up such simulations. The authors are not aware that a similar work had been reported before.

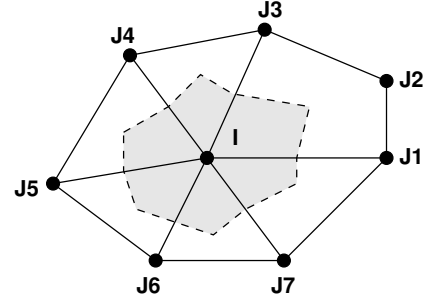


Figure 1: Typical hybrid-cell grid and associated dual mesh.

NUMERICAL MODEL

Governing Equations

The Heat Diffusion equation is solved at the solids [5]

$$\rho c \frac{\partial T}{\partial t} = \nabla \cdot (k \nabla T) + Q, \quad (1)$$

with either Dirichlet, $T = T_w$, or Newmann-like boundary conditions, $-(k \nabla T) \cdot \mathbf{n} = q_w$, at the boundaries, $\partial \Omega$. The heat flux at the wall, q_w , is in general a non-linear function of T and Q is an arbitrary volumetric heat source.

The governing equations are weakly non-linear, because of both the non-linear dependency of the material properties with the temperature, $c(T)$ and $k(T)$, and the boundary conditions, that may include sophisticated correlations.

Spatial discretization

The Heat Diffusion equation in integral form for an arbitrary control volume may be written as

$$\int_{\Omega} \rho c \frac{dT}{dt} d\Omega = \int_{\Sigma} \mathbf{q} \cdot d\mathbf{A} + \int_{\Omega} Q d\Omega, \quad (2)$$

where $\mathbf{q} = k \nabla T$ is the heat flux, Q , the volumetric heat sources, Ω is the solid domain, Σ its boundary and $d\mathbf{A}$ the differential area pointing outward to the boundary.

The solver, known as *Mephisto*, uses hybrid unstructured grids to discretize the spatial domain and may contain cells with an arbitrary number of faces. The solution vector is stored at the vertexes of the cells. The control volume associated to a node is formed by connecting the median dual of the cells surrounding it, using an edge-based data structure (see Fig. 1). For the internal node i ,

the semi-discrete form of the system of non-linear equations (2) can be written, using a finite volume approach, as

$$\rho_i c_i \Omega_i \frac{dT_i}{dt} = \sum_{j=1}^{n_{edges}} \mathbf{q}_{ij} \cdot \mathbf{A}_{ij} + Q_i \Omega_i, \quad (3)$$

where Ω_i is the control volume, \mathbf{A}_{ij} is the area associated to the edge ij , $\mathbf{q}_{ij} = \frac{1}{2}(\mathbf{q}_i + \mathbf{q}_j)$ represents the heat flux through area A_{ij} , and n_{edges} the number of edges that surround node i . The resulting spatially discretized equations can be recast as a summation at each vertex of contributions along all edges meeting at that vertex. The resulting numerical scheme is cell-centered in the dual mesh (dashed line in Fig. 1) and second-order accurate. It may be shown that for triangular grids the scheme is equivalent to a cell vertex finite volume scheme.

Heat fluxes may be evaluated in a number of ways. The gradients of the temperature are approximated at the nodes using also the divergence theorem,

$$(\Omega \nabla T)_i = \sum_{j=1}^{n_{edges}} \frac{1}{2} \mathbf{A}_{ij} (T_i + T_j). \quad (4)$$

Implicit Temporal Discretization

Equation 3 can be expressed in the form

$$(\rho c \Omega)_i \frac{dT_i}{dt} = \mathbf{R}(T). \quad (5)$$

where \mathbf{R} is the residual vector. It is a common practice [6] to use implicit time integration schemes to remove the severe time step limitation of explicit schemes when the diffusion terms are dominant. Equation (5) is then discretized as

$$\frac{(\lambda_i T_i)^{n+1} - (\lambda_i T_i)^n}{\Delta t} = \alpha \mathbf{R}(T^{n+1}) + (1 - \alpha) \mathbf{R}(T^n) \quad (6)$$

where n denotes the time step level and $\lambda = \rho c \Omega$. When $\alpha = 1$ we obtain the backward Euler 1st order scheme while for $\alpha = 0.5$ the 2nd order Crank-Nicholson scheme is obtained, which is preferred for time accurate simulations.

Inner Iteration

The non-linear system of equations represented by Eq. 6 can be linearized as:

$$\frac{U_i^{n+1} - U_i^n}{\Delta t} = \alpha \left(\mathbf{R}(U^n) + \frac{\partial \mathbf{R}^n}{\partial U} \right) (U^{n+1} - U^n) + (1 - \alpha) \mathbf{R}(U^n) \quad (7)$$

where $U = \lambda T$. Writing the equation for all nodes leads to the delta form of the scheme

$$A \Delta U = \mathbf{R}(U^n) \quad (8)$$

where

$$A = \frac{I}{\Delta t} - \alpha \frac{\partial \mathbf{R}^n}{\partial U} \quad (9)$$

and $\Delta U = U^{n+1} - U^n$. When $\Delta t \rightarrow \infty$ and $\alpha = 1$ the Newton scheme to reach the steady state is recovered. The resulting system of linear equations Eq. 8 is solved using the Symmetric Successive Over-Relaxation (SSOR) method. It is a common practice to use a simplified flux version to obtain the left-hand side Jacobian matrix, or directly, as it is our case, to write a simplified version of the Jacobian,

$$\frac{\partial \mathbf{R}^n}{\partial U} \Delta U \simeq \frac{1}{\rho c(\mathbf{x})} \nabla \cdot (k(\mathbf{x}) \nabla (\Delta T)),$$

This effectively means that the material properties, $k(T)$ and $c(T)$, are frozen from the previous step. The non-linearities associated to non-linear boundary conditions, such as convecting or radiating walls, are linearized by freezing the non-linear coefficients. For instance, the heat flux at the wall is linearized as $q_w = h(T_w^n)(T_w^{n+1} - T_w^n)$, but the terms associated to $\partial h / \partial T$ are neglected in the linearization.

Boundary Conditions

Thermal contacts The modelling of a perfect thermal contact between two solids require the use of a conformal mesh. The contact nodes exist at both sides of the contact interface. First the energy equation corresponding to each of the half-volumes associated to every individual node at the interface is written and the fluxes collected and stored. Then the contributions coming from both sides of the interface are sum to form a virtual volume that spans at both sides of the interface. This flux is used to drive the evolution of both nodes. This means that especial care has

to be taken to ensure that nodes at both sides of the interface are ordered consecutively in the SOR scheme.

Thermal contacts with non-null thermal resistance, R , are formulated by computing the local heat flux:

$$q^+ = -q^- = R^{-1}(T^- - T^+). \quad (10)$$

Conformal grids are required also in this case. A virtual edge linking the nodes at both sides of the interface is used to implement this boundary condition. In this case the only caution required -from the point of view of a SOR computation- is to use an updated value of the first node for the second node heat flux. Then, q^+ and q^- will be slightly different during the SOR iterations until convergence.

Infinite cavities Infinite cavities represent large masses of fluid whose thermal capacity is so large that their temperature, T_∞ , is unaffected by the energy exchanged by convection with the surrounding solids. Energy transfer is modelled using Newton's law, $Q_i = A_i h_i (T_\infty - T_i)$. The heat transfer coefficient, h , and the solid temperatures may be local variables.

Voids Voids represent very small closed fluid zones with a infinitely small mass. In this limit, the cavity reaches instantly the equilibrium temperature, T_∞ , with the surrounding solids. As a consequence, the bulk temperature of the cavity is such that ensures that all the heat fluxes exchanged among all the solids in contact with the void balance. If we assume that the energy is exchanged by convection with local HTC's then the cavity fulfills the following relationship:

$$\sum_{boundaries} A_i h_i (T_\infty - T_w^i) = 0. \quad (11)$$

Mass cavities Mass cavities are closed convecting regions with a finite mass, m . At steady state, or if $m \simeq 0$, they behave exactly as voids. The only difference appears in unsteady computations where the mass of the cavity imposes a thermal inertia:

$$m c_v \frac{dT_\infty}{dt} = \sum_{boundaries} A_i h_i (T_\infty - T_w^i).$$

Streams or ducts Streams or ducts consists in a one-dimensional (1D) description of a flow, whose upstream temperature, T_1 , and mass flow, \dot{m} , are known. The enthalpy balance

of the stream with the surrounding walls governs the downstream evolution of the stream temperature, $T_s(s)$:

$$\begin{aligned} \dot{m} c_p \frac{dT_s}{ds} &= Q_{l convection} + Q_{l other sources}, \\ T_s &= T_1 \quad \text{at } s = 0. \end{aligned}$$

The stream is discretized and attached to one or more solid walls. The grid faces of the solids are sliced attending the discretization of the stream segments. At the end of this process, there is a correspondence between stream segments and solids zones (see Fig. 2).

Each stream segment has associated an HTC, which may depend on local wall and/or fluid temperatures. For 3D models it usual to average the wall temperature and the HTC in each stream internal location, using the local wet area, so the equation for the stream becomes:

$$\dot{m} c_p \frac{dT_s}{ds} = A_l \bar{h} (\bar{T}_w - T_s) + Q_{l other sources}, \quad (12)$$

which yields the evolution of the stream temperature.

Discretizing Eq. 12 we obtain,

$$\dot{m} c_p (T_s^{i+1} - T_s^i) = (A_l \Delta s) \bar{h} \left(\bar{T}_w - \frac{T_s^{i+1} + T_s^i}{2} \right) + Q_{other},$$

where i denotes an internal stream node; we can easily isolate $T_s^{i+1}(T_s^i)$. This is stable as far as $\dot{m} c_p > \frac{A_l \bar{h}}{2}$. Otherwise, the less accurate but unconditionally stable form

$$\dot{m} c_p (T_s^{i+1} - T_s^i) = A_l \bar{h} (\bar{T}_w - T_s^{i+1}) + Q_{other}$$

is used. Q_{other} is used to model the stream viscous dissipation or any other heat source

At unsteady computations, streams are assumed to behave quasi-steadily, as it is the case of the cooling flows in a turbine operating in transient conditions. This is realistic for gas turbines, since the stream residence time is much smaller than the diffusion time of the solid.

Fluid network definition Streams can be mixed using a mass an enthalpy balance at the mixing point to derive the initial conditions of the downstream stream. In practice, a sort of fluid

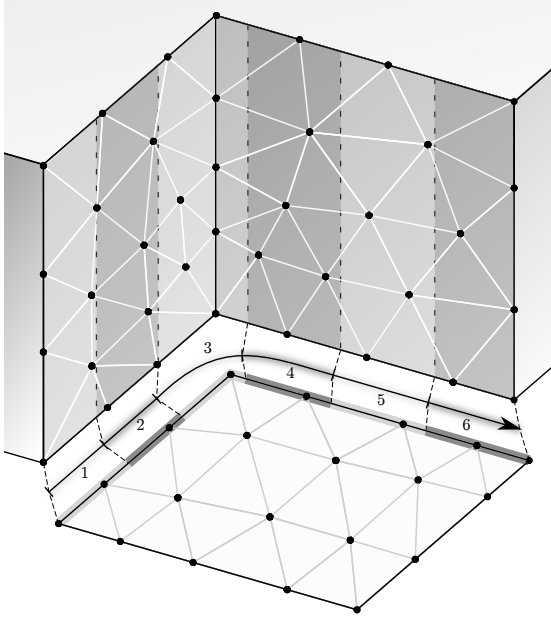


Figure 2: Sketch of a duct with six internal segments, attached to a group of faces from a 3D solid and to the edge of a 2D solid . The stripes of the surface mesh mark the correspondence with internal duct stations.

network linked to the solid model is defined. To solve the fluid network, we keep updating the mixed variables at each of the SOR iterations. This procedure has shown to be robust enough, but it is worth noting that the sense of the streams must be defined beforehand.

Following the SOR philosophy, mixing is performed as soon as the information of the streams to be mixed is available, providing an updated boundary condition for the downstream duct. In fact, streams are ordered in terms of the mixing conditions because of this reason. When circular references exist, some of the streams cannot use updated values, so they use the values of the previous iteration.

Finally, a stream can discharge into a void, contributing with its enthalpy to the energy balance of the void,

$$\sum_{boundaries} A_i h_i (T_w^i - T_\infty) + \dot{m} h_{stream}(T_d) = 0 \quad (13)$$

where T_d is the discharge temperature of the stream. Conversely, a stream could depart from a void or a mass cavity.

Radiative heat transfer The thermal power emitted by a perfect diffuse radiating gray boundary [5] is

$$\dot{q}_{emitted} = A \epsilon \sigma T_w^4,$$

being ϵ the emissivity which is considered constant. The boundary i will intercept radiation emitted by any of the other boundaries j ,

$$\dot{q}_{intercepted} = \sigma \sum_j A f_{i \rightarrow j} \epsilon_j T_j^4.$$

where $f_{i \rightarrow j}$ is the corresponding view factor. Gray bodies reflect a fraction $1 - \epsilon$ of all the received energy. These reflections are intercepted again, and the $1 - \epsilon$ part of these interceptions is reflected again and so on.

The net radiating flux at each boundary, depends at the end on all the radiating boundaries. This flux may be written as:

$$\dot{q}_{net} = \sigma A \left(\overline{f \epsilon} \overline{T}^4 - \overline{\epsilon} T_w^4 \right), \quad (14)$$

where the rebounds effect is properly taken into account at $\overline{T}(T_j, \epsilon_j, f_{i \rightarrow j})$, where $\overline{f \epsilon}(\epsilon_j, f_{i \rightarrow j})$ and $\overline{\epsilon}(\epsilon_j, f_{i \rightarrow j})$ are constant values. Computing \overline{T} , $\overline{f \epsilon}$ and $\overline{\epsilon}$ is equivalent to solve the gray body problem.

The neat radiative heat flux (Eq. 14) is linearized as follows. Firstly we express the flux as

$$\dot{q}_{net} = \sigma A \left((\overline{f \epsilon} - \overline{\epsilon}) \overline{T}^4 + \overline{\epsilon} (\overline{T}^4 - T_w^4) \right). \quad (15)$$

Then, we use the temperatures of the previous iteration to compute \overline{T} mean. The first term of Eq. 15 is frozen at the present iteration. The computation of the heat flux at iteration $n + 1$ is then linearized as

$$\begin{aligned} \dot{q}_{net}^{n+1} = & \sigma A \left((\overline{f \epsilon} - \overline{\epsilon})^n (\overline{T}^4)^n \right. \\ & \left. + \overline{\epsilon} (\overline{T}^2 + T_w^2)^n (\overline{T} + T_w)^n (\overline{T} - T_w)^{n+1} \right). \end{aligned} \quad (16)$$

The computation of the view factors, $f_{i \rightarrow j}$, is expensive for cases with a large number of surface elements [7]. The problem is not the computation of the view factor itself but the checking of the shapes generated by other elements located between the node i and the node j , which has a computational cost which is $O(n^3)$, where n is the number of radiating boundaries. However, for axisymmetric geometries, it is possible to devise algorithms that exploit this symmetry [8] to reduce the computational cost by several orders of magnitude.

INTERFACE PLANE TREATMENT

Introduction

Turbomachinery simulations are quite often based on the use of reduced order models. These models are usually based in some sort of mixing or averaging process in the circumferential direction. The most classical example may be seen in multi-row aerodynamic simulations, where the flow is averaged or mixed in the interface between different rows, to remove unsteady effects and allow the transfer of information between rows with different pitches. The averaging process usually enforces that conservation laws are fulfilled across the interface.

Enforcement of the conservations laws requires that across the selected interface

$$\int_{\Sigma} \mathbf{F}(\mathbf{U}^-, \nabla \mathbf{U}^-) \cdot d\mathbf{A} = \int_{\Sigma} \mathbf{F}(\mathbf{U}^+, \nabla \mathbf{U}^+) \cdot d\mathbf{A} \quad (17)$$

where \mathbf{F} is the flux vector, that in general is a non linear function of the vector of conservative variables, \mathbf{U} , and its gradient, $\nabla \mathbf{U}$. When the gradients are neglected in the interface, as it is usually the case in the solution of the Navier-Stokes equations, Eq. 17 provides a relation between the variables at both sides of the interface. For the 1D Euler equations Eq. 17 becomes the Rankine-Hugoniot relationship. When the downstream flow is uniform Eq. 17 becomes $\int_{\Sigma} \mathbf{F}(\mathbf{U}^+) \cdot d\mathbf{A} = \mathbf{F}(\mathbf{U}^+) \cdot A_n$ and determines the mixed-out state.

Laplace equation, although significantly simpler than the Navier-Stokes equations, presents some particularities related with the averaging process. The flux-vector is a scalar since we only deal in this case with the energy equation, actually $\mathbf{F} = \mathbf{q} = k\nabla T$. This means that on the contrary than the standard case in fluid-dynamics, $\mathbf{F} = \mathbf{F}(\mathbf{U}, \nabla \mathbf{U})$, since the gradient of the variables can not be neglected. It is important to observed that if the conductivity is constant, $k = k_0$, Eq. 17 only provides a relationship between the gradients at both sides of the interface, what is not enough to determine the solution.

The conservation law across the interface (Eq. 17) reduces in this case to

$$\int_{\Sigma} \mathbf{q}(T^-) \cdot d\mathbf{A} = \int_{\Sigma} \mathbf{q}(T^+) \cdot d\mathbf{A} \quad (18)$$

which basically states that the total heat flux across the interface is constant. Some degree of modelling is needed to fix the condition that should satisfy the temperature. In a perfect contact the temperature at both sides of the interface is point to point the same, i.e.: $T^- = T^+ \forall \mathbf{x}$ at Σ . This automatically suggests that if we consider a circumferential average state, \bar{T}^- at Σ^- , then

$$\int_{\Sigma^-} T^- dA = \bar{T}^+ A \quad (19)$$

which essentially requires that the mean temperature is conserved across the interface.

Duct-Void Concept

With the aim of easing the implementation of the aforementioned ideas we introduce the concept of duct-voids, which is nothing else than a 1D concatenation of voids. The main idea is to satisfy Eqs. 18 and 19 by forcing to both sides of the interface to exchange heat by convection against a virtual cavity with zero mass. Duct-voids are similar to streams/ducts from the pre-processing point of view; this means that each duct-void internal segment has a correspondence with several solid zones (see Fig. 2). Solving a duct-void consists in obtaining the local temperature of the void, T_{∞}^i , which balances the total heat flux received locally:

$$\forall i, \sum_{j \in \text{segment } i} A_j h_j (T_{\infty}^i - T_w^j) = 0. \quad (20)$$

Note that in this case segments are totally independent, and a duct-void behaves as a group of *independent* voids. As it is discussed below, duct-voids may be used for several purposes.

Modeling 2D/3D interfaces using duct-voids Setting up a duct-void with two branches, each of it attached to a solid wall, is equivalent to define a thermal contact with a thermal resistance, as can be derived by direct comparison of Eqs. 10 and 20.

The main advantage of using a duct-void instead of a thermal contact is that the duct-void entity does not require a conformal mesh (the pre-processing stage has split the solid faces into the slices required by each duct-void segment -see Fig 2-). As a result, a resistive contact can be defined between the 3D and Q3D solids. It can also be used to define a three-component, or even a n -component, contact if it is required. On the other hand, a duct-void cannot model a perfect contact since the use of very small thermal resistance spoils the solver convergence.

The use of duct voids to transfer information between the 3D and 2D sides ensures that the heat flux is locally balanced. The local HTC is a degree of freedom. If the HTC is very large, the contact is nearly perfect and the duct void tends to smooth the azimuthal temperature distribution at the 3D side of the contact (i.e.: in the stripes direction at Fig. 2). This effect could be potentially corrected computing the wall temperature average for each side,

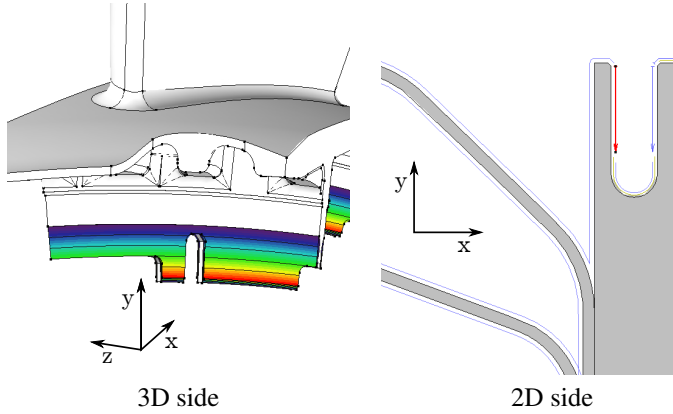


Figure 3: Scheme of a duct-void set-up between a 3D model face (left) and a 2D model segment used to model a thermal contact (right).

and using that temperature to impose the heat flux in the solid wall, instead of the local temperature.

Figure 3 shows the internal representation parameter contour lines of a 3D face with a duct-void attached to it and the matching branch at the 2D side.

It is worth noting that plain voids can also model thermal contacts but the heat flux is averaged along the contact. Solid wall temperatures are smoothed out at the contact zone. Duct-voids retain a one dimensional spatial variation of the contact phenomenon, which is a good approach when combining Q3D and 3D models.

Scaling factors Setting up a contact between 3D and axi-symmetric models requires a scaling of the fluxes either at the 2D or the 3D side. Three-Dimensional models cover a certain pitch, whereas axi-symmetric models cover either the whole circumference or an arbitrary pitch. In order to fix this problem a scaling factor, m_j , is specified at each convective condition affecting only to the duct-void energy equation -not the solid part-. This means that the energy balance equation for the duct void (Eq. 20) is modified as:

$$\forall i, \sum_{j \in \text{segment } i} m_j A_j h_j (T_\infty^i - T_w^j) = 0, \quad (21)$$

whereas the solid is *still* receiving the heat flux $Q = A_j h_j (T_\infty^i - T_w^j)$.

Scaling factors are usually set to $2\pi/\text{pitch}$ on the 3D side, and to 1 at the 2D/Q3D side. This practice ensures that energy is conserved in the contacts between 2D and 3D models, while the averaged temperature difference is controlled by the HTC level.

Scaling factors are also necessary at ducts and voids attached to both 2D and 3D models.

Temperature transfer between 2D and 3D models

Duct-voids may be also used as a mechanism to transfer a temperature distribution from a 3D model, usually a circumferential variation, into a 2D representation of the same model. If the scaling factor is set to zero at one of the sides, the equilibrium temperature of the duct void, T_∞^i , becomes the weighted area average of the temperatures of the other side:

$$T_\infty^i = \frac{1}{A_T} \sum_{j \in \text{segment } i} A_j T_j \quad (22)$$

The side at which the scaling factor is set to zero is heated by convection against this temperature.

A 2D (axi-symmetric) approximate representation of a 3D model at the Q3D part may be used to compute radiative heat transfer in a simplified way to reduce the computational time. Another use is the later computation of thermo-mechanical displacements with a pure Q3D model. When using a 2D representation, it is important that the represented part needs to be thermally decoupled from the rest of the Q3D model; otherwise the heat transfer of the component would be accounted for twice.

When a scaling factor of zero is used at the 2D side to prescribe the average temperature distribution of a detailed 3D model, it is convenient to use a low HTC at the 3D branch and a high one at the 2D one. In one hand, the low HTC at the 3D branch (strictly speaking $hL_c/k_s \gg 1$, where L_c is the characteristic length in the normal direction to the wall) ensures that the duct-void reaches locally the azimuthal average of the 3D temperatures without altering the 3D temperature distribution. On the other hand, a large HTC at the 2D branch (strictly speaking $hL_c/k_s \gg 1$), ensures the temperatures at the 2D are the same than that of the duct-void internal representation, T_∞ , which is nothing else that the azimuthal average of the temperatures of the 3D model.

APPLICATION EXAMPLE

The aforementioned modeling techniques have been applied to the thermal analysis of a two-stage turbine. The actual model is quite complex and it will not be described here in full detail for the sake of brevity. The model consists of a Q3D model of the whole turbine and 3D sub-components of the rotor blade and stator vanes which may be linked to the Q3D model in different ways. In this case only the the first vane -which has active cooling- has been replaced by a 3D component.

The refrigeration effect was not properly included in the original model (which consisted in a Q3D model of the whole turbine, plus a 3D detail model of the vane using boundary conditions extracted from the results of the Q3D model). The cooling effect could have

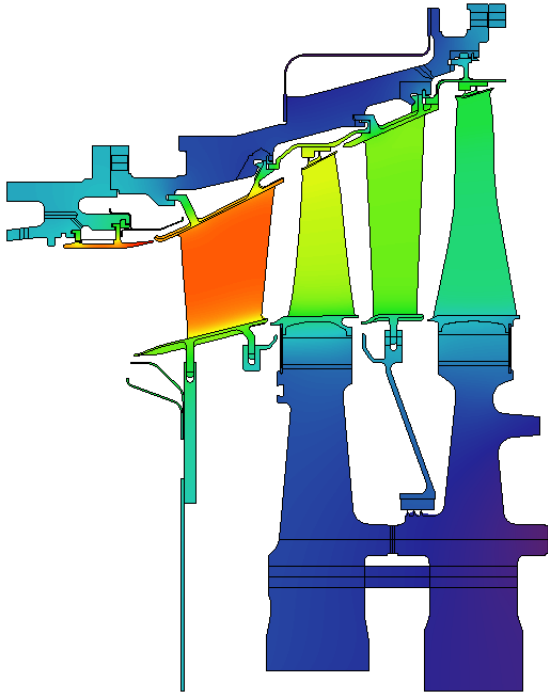


Figure 4: Baseline Q3D model temperature distribution.

been modeled at the original Q3D model using simplifications, certain hypothesis and some tricks. With the use of a combined 2D/3D model, these simplifications and uncertainties are reduced.

Baseline uncoupled model

Figure 4 shows the baseline Q3D model. Essentially all the components are axi-symmetric except the airfoils, which are modeled as two-dimensional objects with an equivalent thickness. Contacts and radiation among different components have been specified, but they are not described here since this is not the main purpose of this work. Solids have as well convection against cavities and different types of streams, being the HTC correlations embedded in the software. A close-up of one of the zones of interest because of the coupling effects is shown in Fig. 5. Figure 6 shows the first NGV 3D model and temperature contours, whose boundary conditions have been extracted from the global Q3D. The NGV is hollow and may be cooled, but cooling has not been included neither in the Q3D nor in the 3D model.

The so-called standard procedure consists in constructing a Q3D model of the whole turbine including the maximum amount of information related with convection and radiation, and then use these temperatures as BCs for the 3D models.

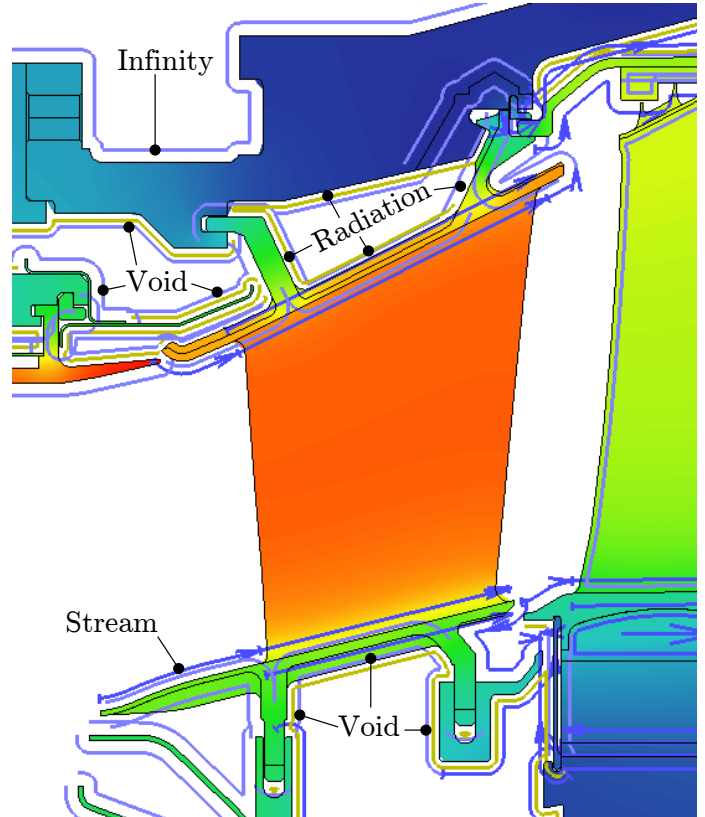


Figure 5: Detail of the boundary conditions around the refrigerated vane. Blue lines: convection ; arrows are used where streams or ducts are attached. Yellow lines: internal radiation

Coupled model

Conduction and Convection Treatment The basic idea behind the coupled model is to increase the accuracy of the predictions by using a model of higher fidelity. It is assumed that the use axi-symmetric models for casings, disks, etc., is a cost effective approach, while it is acknowledged that fully 3D models are required for rotor blades and vanes packets, for instance. It is considered that a model that could link global Q3D models and detail 3D models in an effective way, would be optimum from a practical point of view. The coupled model, on the contrary than the standard practice, supports a bidirectional coupling between the Q3D and the 3D models, and allows a native support for transients. At transients, the equivalent thickness approximation of a Q3D model may not be able to properly reproduce the behaviour of a hollow blade, which depends on the local thickness, rather than on the total mass (i.e. the total thickness). Moreover the coupled approach provides feedback to the global Q3D model of the information collected from the 3D models.

The information transfer between Q3D and 3D models it is not obvious since both models are computed simultaneously and convection and radiation are present. Therefore some modeling

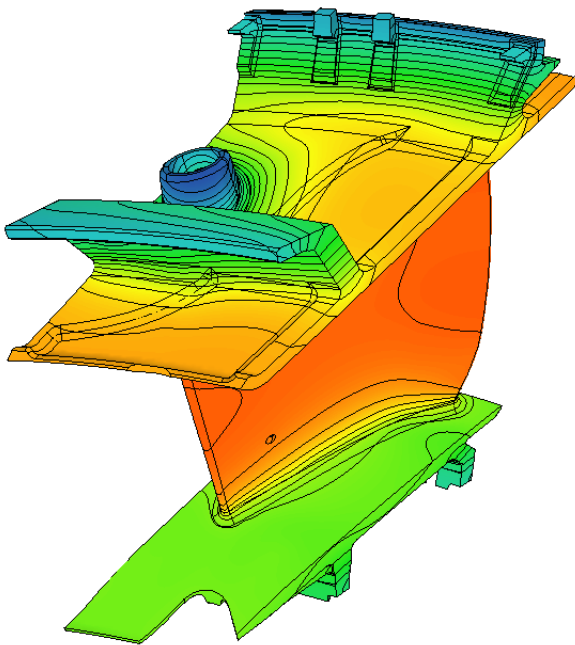


Figure 6: Vane temperature distribution obtained using the boundary conditions derived from the baseline uncooled Q3D model.

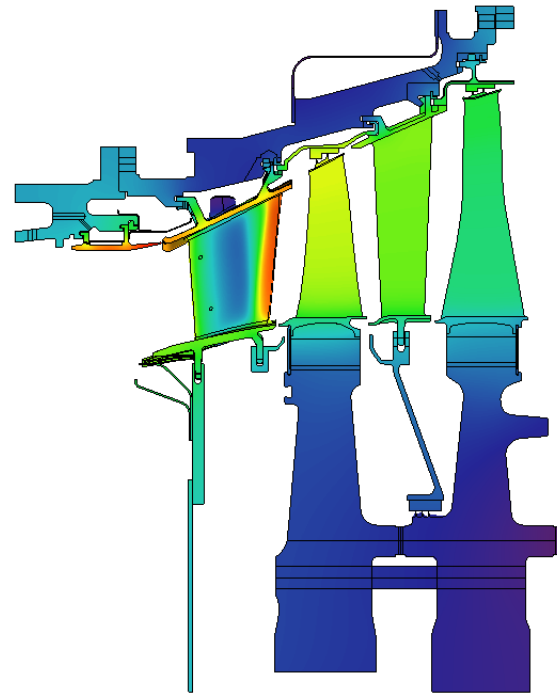


Figure 8: The coupled model, with the 3D NGV and the Q3D rest of the turbine.

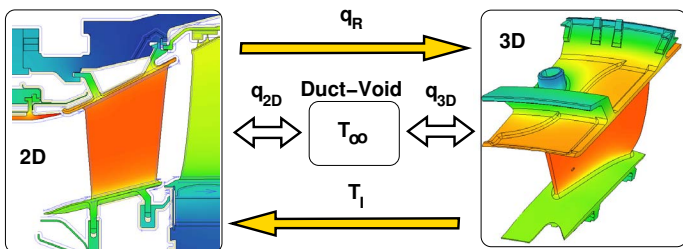


Figure 7: Coupling scheme of the 2D and 3D models. White: Convection and conduction scheme. Yellow: Radiation scheme

decisions need to be made. We will use the 1st vane of the turbine as a demonstrator of the new approach, because of its capability to include internal cooling, that certainly has an added difficulty for its modeling in a Q3D environment.

The vane is now computed using a 3D sub-model, and all the convective boundary conditions that were applied in the 2D counter part model have been moved to the 3D model. It is important to pay attention to the contacts between the Q3D and the 3D models. The rest of boundary conditions are a direct translation. The modeling of the heat exchange between the airfoil and the main flow-path, for instance, existed in both models and is conceptually the same, although obviously much more detail could be included in the 3D case by for instance importing the HTC's from a CFD

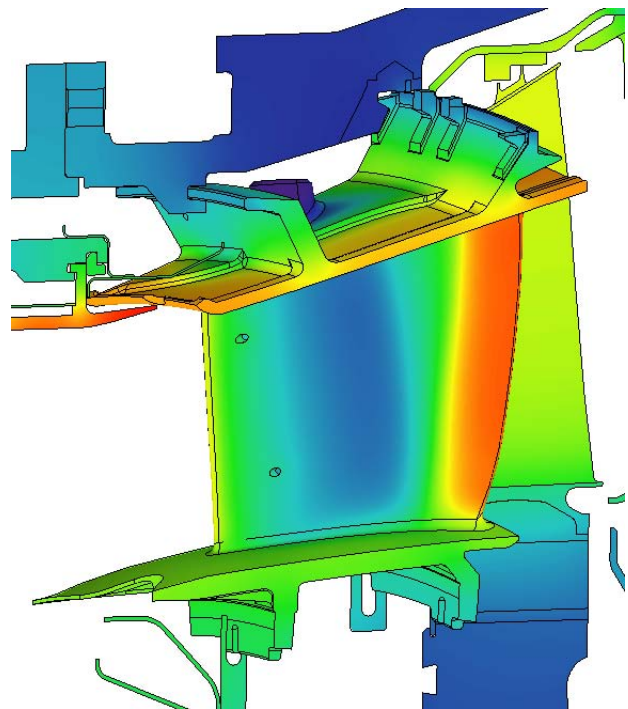


Figure 9: Detail of the solution of the coupled model at the NGV zone, where active cooling has been modeled.

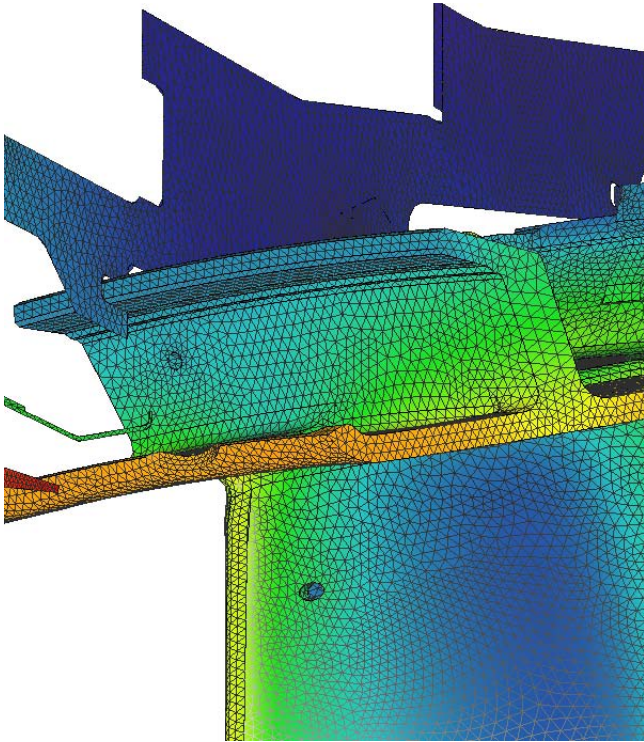


Figure 10: Detail of the grid used for the coupled model, showing one of the zones where a 2D-3D contact is modeled with a duct-void.

model. Contacts at the two rails of the hook (at the tip of the airfoil) and at the four faces of the seal contacts (at the hub of the airfoil), are modeled using duct-voids between the 3D faces of the vanes and the segments of the 2D models. Scaling factors are used at the 3D side to ensure energy conservation at these interfaces.

At this point, the 2D counterpart of the vane could be removed from the 2D model, but instead the 2D approximation of the vane is kept. Nevertheless, its conductive and convective BCs have been removed, since only the contributions coming from the 3D model are trusted. In the absence of radiation this is equivalent to removing the vane from the 2D model.

Radiation Treatment When radiation effects need to be retained, the situation is somewhat more complex. This is the case in our problem in the cavity defined by the outer annulus of the flow-path, the external casing and the hooks that support the vane. In this cavity the convection velocity is due to small leakages and convection and radiation can be comparable.

Radiating conditions of the 2D model (internal radiation with the turbine case on top and the turbine disk at the bottom) are however kept. Therefore, at these radiating faces, the temperature distribution obtained from the 3D vane is prescribed in the 2D model,

in order to compute the net flux associated to the radiation. The turbine casing and the rest of the Q3D model sees the 3D model temperature distribution on the 2D vane geometry. Then, the radiative heat transfer will be correctly computed, but under the limitations of the assumption that the geometry is axi-symmetric. This approximation can be taken into account to compute the view factors in a very efficient way [8, 7]. This approach is good compromise, since it allows to take into account radiation effects in the whole turbine, retain 3D conduction and convection effects in complex parts and avoid a fully 3D computation of the radiation in the whole turbine, that could be not practical in terms of CPU time.

Using this approach, the cavity above the vane will receive a precise radiative heat transfer balance with the 3D model, including radiation. The radiation heat flux at the 3D model may be simplified by emitting against a virtual external infinity, at the average of the temperature for the 2D radiating zone. This is a reasonable hypothesis in this case since the cavity closure is almost perfect and the shape of the vane top is convex in the major part of its extent. This is also a standard inexpensive method at 3D detail thermal models. Alternatively the radiative heat flux from the 2D vane counterpart could be collected, which is certainly a more consistent approach.

RESULTS

Two different cases for the whole turbine have been simulated to compare the coupled and uncoupled approaches. The sole difference is the presence of a cooling flow or not in the cooling passage of the first NGV. Figures, 4 and 5 present the temperature distribution of the baseline case when cooling is not considered.

Uncoupled models

Figure 11 shows the temperature difference between the uncoupled and coupled models for this case. There are important differences at the vane contacts, at the vane top and at the casing zone above the vane. At the contacts the highest differences are found, because the uncoupled model is not consistent; the heat flux obtained at the 3D vane with the temperature specified at the contact zone is different from that found at the Q3D model. These inconsistencies come from the geometric differences between the Q3D and the 3D vane, and the different sets of boundary conditions used in the 2D and 3D models.

These inconsistencies are avoided in the coupled model, where the heat flux is conserved at the interface and the temperature jump controlled. In this case the temperature at the contacts is lower for the coupled approach.

The uncoupled model has simplified HTC's imposed on the top of the vane which cause the differences of about 7K at that zone. There, differences are in average negative (even though there is a

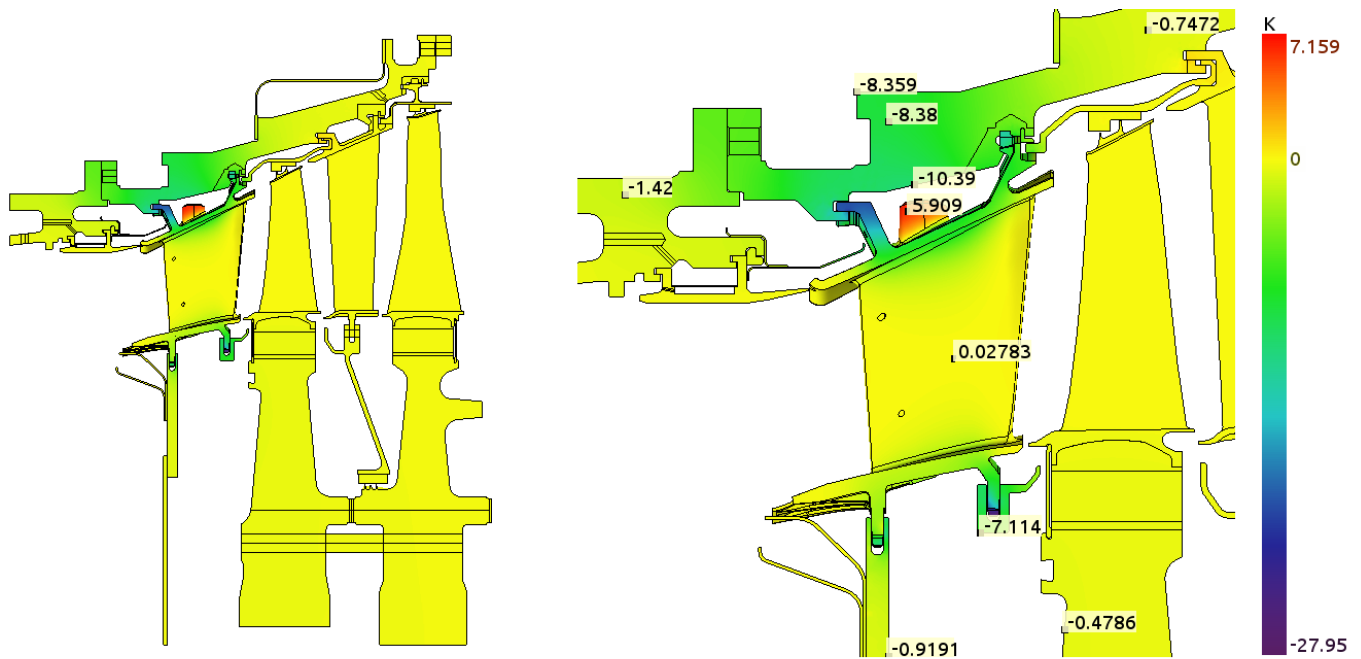


Figure 11: Temperature difference for the coupled and uncoupled approaches, $T_{coupled} - T_{uncoupled}$, for the uncooled case. Left: view of the turbine layout. Right: close-up of the zone of interest.

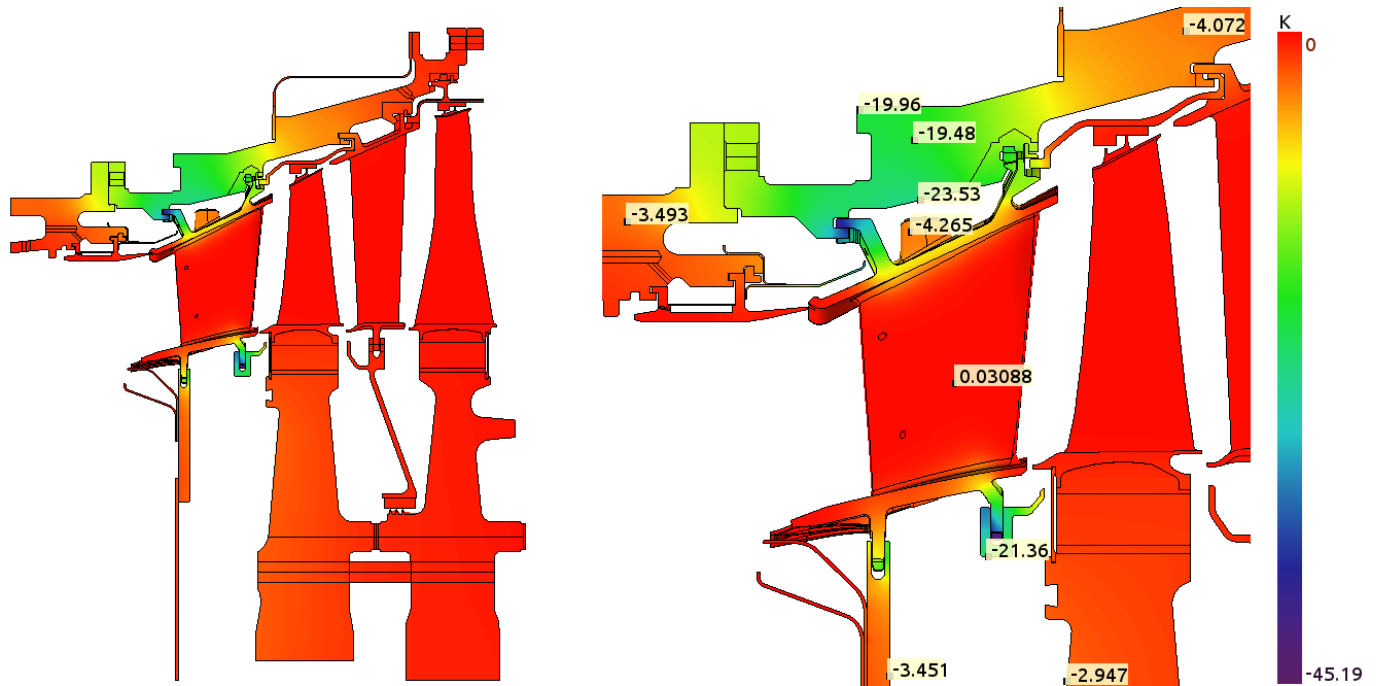


Figure 12: Difference of temperatures between the coupled and uncoupled models, $T_{coupled} - T_{uncoupled}$, for the cooled case. Left: layout view. Right: detail of the zone of interest.

positive hot spot), and the coupled model has a lower radiating interaction with the casing. Because of these facts, and the colder temperature at the contacts, the temperature of the casing at the zone on top of the vane is about 10K colder at the coupled model. The vane temperature at the flow-path region is very similar in both cases, because, there, the HTC is very high and the behavior is controlled by the stagnation temperature of the main flow-path.

Cooled Models

In the second case, the cooling effect of the passage has been modeled using a stream with an HTC correlation, in both coupled and uncoupled 3D vanes flowing through the main cooling hole. The stream definition is the same in both coupled and uncoupled 3D models.

Coupled model results are shown for this case at the Figs. 8-9. Since the uncoupled 2D model is not aware of this cooling, bigger differences are found (see Fig. 12). Differences at the top of the vane are lower in this case because that zone is controlled by the cooling flow. The contact temperature jump has increased notably, because the uncoupled models are more inconsistent now. The casing differences are now bigger, of about 20°C, in the top of the vane. This difference is about a 3% of the range between flow path and the cooling flow temperatures. At the coupled case, the heat conducted from the vane to the casing is now lower because of the cooling. Also, the radiative effect is lower because the vane top is colder. Similar differences, but in a smaller scale, are found at the bottom zone of the vane, also because of these reasons.

COMPUTATIONAL COST

The axisymmetric view factors computation requires about 14 seconds using an Intel Core 2 Duo T7200@2GHz CPU. The 3D standalone model mesh has 44,000 nodes and requires 17 seconds to be converged, after 490 SOR iterations. The Q3D standalone model, with 21,000 nodes, requires 3,000 iterations and takes 26 seconds to be converged. The coupled model, needs about 182 seconds to be converged, requiring 3240 iterations. The coupled approach needs more than four times CPU time than the uncoupled approach.

The computational cost of the coupled model is large compared to the uncoupled models. The reason for this is that the 3D sub-components are reaching the local equilibrium quickly during the SOR evolution because their HTCs are large. The 2D global model has, however, zones with weak heat fluxes imposed by the local boundary conditions. These regions need more iterations to converge. Also, the 2D model covers a much larger domain, what leads as well to longer characteristic times. Since 3D model has more nodes than the 2D one, there is a noticeable penalty due to the larger number of iterations induced by the 2D model on

the 3D sub-component. The coupled approach is still interesting because the required time for convergence is still small in absolute terms.

CONCLUSIONS

Axi-symmetric Q3D models are very useful to predict the temperature distribution of a gas turbine, since they allow a cost-effective multi-component modelling of the whole turbine. Radiative heat transfer computation is affordable for Q3D models, whereas it is significantly more expensive at 3D models. On the other hand, thermal models require of intensive modeling of cooling and sealing flows, due to the complexity and cost associated to their simulation within the current design timescales.

A thermal solver which deals with this intensive modeling has been briefly outlined. The solver was initially conceived to simulate either Q3D or 3D models. A new methodology to create mixed models which contain both Q3D and 3D sub-components has been described. The method has been successfully used to link a 3D cooled NGV with a Q3D model of the whole. Differences of up to 3% of the temperature range between the flow path and cooling flow temperatures have been found with the baseline model (that first computes the whole turbine and, then, uses the temperatures at the interfaces between 2D and 3D model as boundary conditions). These differences may be important from an engineering point of view.

The logistics of the coupled approach is easier for the designer, especially for transient calculations, since many manual operations are removed and are handled in a transparent way by the system. As a consequence the coupled approach is less prone to errors.

ACKNOWLEDGEMENTS

The authors wish to thank ITP allowing the publication of this paper.

REFERENCES

- [1] Verdicchio, J. A., Chew, J. W., and Hills, N. J., 2001. "Coupled fluid/solid heat transfer computation for turbine discs". In ASME Paper No. 2001-GT-012.
- [2] Kusterer, K., Bohn, D., Sugimoto, T., and Tanaka, R., 2004. "Conjugate calculations for a film-cooled blade under different operating conditions". In ASME Paper No. GT2004-53719.
- [3] Verstraete, T., Alsalihi, Z., and den Braembussche, R. A. V., 2006. "Numerical study of the heat transfer in micro gas turbines". In ASME Paper No. GT2006-90161.
- [4] Armstrong, I., and Edmunds, T., 1989. "Fully automatic analysis in the industrial environment". *Proceedings of 2nd International Conference on Quality Assurance and Standards, NAFEMS*.

- [5] Incropera, F., and Dewitt, D., 1985. *Introduction to heat transfer*. John Wiley and Sons Inc., New York, NY, 1 Feb.
- [6] Press, W. H., Teukolsky, S. A., Vetterling, W. T., and Flannery, B. P., 2002. *Numerical Recipes in C++ - The Art of Scientific Computing - Second Edition*.
- [7] Ashdown, I., 1994. *Radiosity: A Programmer's Perspective*. John Wiley & Sons, Inc., New York, NY, USA.
- [8] Naraghi, M. H. N., and Nunes, E. M., 2002. "Effects of gas radiation on the thermal characteristics of regeneratively cooled rocket engines". *ASME Conference Proceedings*, **2002**(36347), pp. 145–154.